

# Cation effect on the electrochemical reduction of polyoxometalates in room temperature ionic liquids<sup>†</sup>

 Juliette I. Phillips<sup>A</sup>, Shinya Azuma<sup>A,B</sup>, Junqiao Lee<sup>A</sup> , Tadaharu Ueda<sup>C,D</sup> and Debbie S. Silvester<sup>A,\*</sup> 

For full list of author affiliations and declarations see end of paper

**\*Correspondence to:**

 Debbie S. Silvester  
 School of Molecular and Life Sciences,  
 Curtin University, GPO Box U1987, Perth,  
 WA 6845, Australia  
 Email: [d.silvester-dean@curtin.edu.au](mailto:d.silvester-dean@curtin.edu.au)
**Handling Editor:**

Curt Wentrup

**Received:** 20 June 2022

**Accepted:** 22 September 2022

**Published:** 22 November 2022

**Cite this:**

 Phillips JI et al. (2022)  
*Australian Journal of Chemistry*  
**75**(11), 865–876. doi:[10.1071/CH22140](https://doi.org/10.1071/CH22140)

© 2022 The Author(s) (or their employer(s)). Published by CSIRO Publishing.

 This is an open access article distributed under the Creative Commons Attribution-NonCommercial-NoDerivatives 4.0 International License ([CC BY-NC-ND](https://creativecommons.org/licenses/by-nc-nd/4.0/))

OPEN ACCESS

**ABSTRACT**

Polyoxometalates (POMs) are compounds that undergo multiple successive one-electron redox transitions, making them convenient model reactants to study ion solvation effects. Room temperature ionic liquids (RTILs) are solvents made entirely of ions, and are expected to have interactions with the highly negatively charged POM reduction products. In this work, 12 RTILs with a range of different anions ([FSI]<sup>−</sup>=bis(fluorosulfonyl)imide, [TFSI]<sup>−</sup>=bis(trifluoromethylsulfonyl)imide, [BETI]<sup>−</sup>=bis(pentafluoroethylsulfonyl)imide, [BF<sub>4</sub>]<sup>−</sup>, [PF<sub>6</sub>]<sup>−</sup>) and cations (imidazolium, pyrrolidinium, sulfonium, ammonium, phosphonium) were employed as solvents to study the kinetics and thermodynamics of [S<sub>2</sub>W<sub>18</sub>O<sub>62</sub>]<sup>4−</sup> reduction, to shed light on solvation effects and ion-pairing effects caused by different RTIL structures. Up to six reversible reduction processes (producing highly negatively charged [S<sub>2</sub>W<sub>18</sub>O<sub>62</sub>]<sup>10−</sup>) were observed. For the RTILs that showed multiple processes, a clear trend in both the thermodynamics (inferred from the reduction peak potentials) and kinetics (inferred from the peak-to-peak separation) was observed, in the order: imidazolium < sulfonium ≈ ammonium < pyrrolidinium < phosphonium, supporting strong interactions of the negatively charged POM reduction products with the cation. Two related POMs, [P<sub>2</sub>W<sub>18</sub>O<sub>62</sub>]<sup>6−</sup> and [PW<sub>12</sub>O<sub>40</sub>]<sup>3−</sup>, were also studied in the optimum RTIL found for [S<sub>2</sub>W<sub>18</sub>O<sub>62</sub>]<sup>4−</sup> ([C<sub>2</sub>mim][FSI]=1-ethyl-3-methylimidazolium bis(fluorosulfonyl)imide), revealing fast kinetics and asymmetric peaks for [PW<sub>12</sub>O<sub>40</sub>]<sup>3−</sup>. This work demonstrates the importance of understanding the solvation effects of RTIL ions for highly charged electrogenerated products, allowing tuning of the RTIL structure to achieve the optimum kinetics and thermodynamics for an electrochemical process.

**Keywords:** cation, cyclic voltammetry, electrochemistry, ionic liquids, ion-pairing, polyoxometalates, reduction, solvation.

**Introduction**

Polyoxometalates (POMs) are ionic metal oxide clusters that consist of so-called hetero atoms such as sulfur, phosphorus and silica, addenda atoms, such as molybdenum and tungsten, and oxygen with a variety of structures. Keggin-type POMs, [XM<sub>12</sub>O<sub>40</sub>]<sup>n−</sup> (X = S, P, Si, etc.; M = Mo, W) and Wells–Dawson type POMs, [X<sub>2</sub>M<sub>18</sub>O<sub>62</sub>]<sup>n−</sup>, have been extensively investigated from fundamental and practical points of view.<sup>[1–4]</sup> Fig. 1 shows the polyhedral representation of the structure of (a) Keggin-type, and (b) Wells–Dawson-type POMs. Many POMs can accommodate and release multiple electrons while retaining their structures (e.g. see electrochemical reaction scheme for a typical POM reduction in Fig. 1c). Studies on the electrochemical behaviour of POMs in aqueous solutions, organic solvents and mixed media have provided the following general observations: (1) the acidity of the electrolyte solution greatly affects the voltammetric behaviour of POMs; at each reduction step, a one-electron transfer occurs under neutral conditions where no proton is coupled, whereas a two-electron transfer step occurs under

<sup>†</sup>(Invited contribution for the special issue RACI/AAS Awards). Debbie S. Silvester was awarded the RACI Physical Chemistry Lectureship from the Physical Chemistry Division.

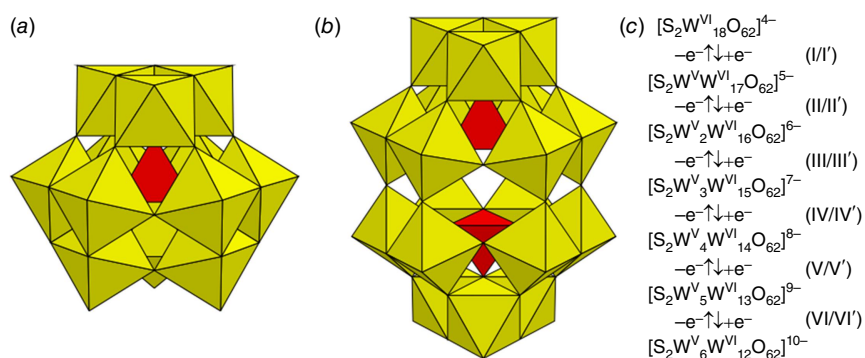


**Fig. 1.** (a) Keggin, and (b) Wells–Dawson structures of POMs, and (c) redox transitions for the electrochemical reduction of  $[S_2W_{18}O_{62}]^{4-}$ . Yellow:  $MO_6$  unit (where M = Mo, W). Red:  $XO_4$  unit (where X = Si, P, S).

highly acidic conditions.<sup>[5,6]</sup> (2) The redox potential for the first reduction process of Keggin-type POMs under neutral conditions is linearly related to the total ion charge and bond length of  $W-\mu_4O$  where the oxygen is bound to the central (hetero) atom.<sup>[7,8]</sup>

Room temperature ionic liquids (RTILs) have been widely investigated as combined solvent/salt systems owing to their non-volatility and high conductivity,<sup>[9–13]</sup> which are also very important properties for the synthesis and electrochemistry of POMs. The appropriate selection of solvent is one of the key factors required to prepare POMs in high yield and with high selectivity. For example, novel POM  $[WFe_9(\mu_3-O)_3(\mu_2-OH)_6O_4H_2O(SiW_9O_{34})_3]^{17-}$  and POM-based metal–organic frameworks  $(n-Bu_4N)_2[Cu^{II}(BBTZ)_2(Mo_8O_{26})]$  (BBTZ = 1,4-bis(1,2,4-triazol-1-ylmethyl)benzene) have been synthesised in 1-ethyl-3-methylimidazolium bromide ( $[C_2mim]Br$ ) under isothermal conditions.<sup>[14,15]</sup> Even IL-based POMs – which are categorised based on their glass transition temperature ( $T_g$ ); where  $T_g < 100^\circ C$ , they are called POM-ILs, and  $T_g > 100^\circ C$ , they are called IL-POMs – have been prepared by simple synthesis methods using large-sized organic cations such as trihexyl(tetradecyl)- or tributyl(hexadecyl)-phosphonium cations, tetra-*n*-octyl-ammonium cations and imidazolium-based cations.<sup>[16]</sup> They exhibit fascinating chemical properties: reversible conversion between the glass phase and the liquid phase, solvent-free catalysis for alcohol oxidation and epoxidation of olefins, anticorrosion and water treatment to remove  $Cd^{2+}$  and  $Pb^{2+}$ .<sup>[16]</sup>

Moreover, the electrochemical behaviour of POMs dissolved in RTILs, as well as POMs mechanically attached on the surface of electrodes with RTILs as conductors, has been also investigated to obtain redox potentials and diffusion coefficients. The RTIL solvents studied have been mostly imidazolium cation-based RTILs, in addition to a pyrrolidinium cation and also a distillable liquid  $[Me_2NH_2]^+ [Me_2N-CO_2]^-$ .<sup>[17–19]</sup> Because most POMs possess low surface charge density and high symmetry, with no solvent molecule directly bound to the POMs, they are excellent probes to investigate the chemical properties of solvents, similar to tetraphenylarsonium tetraphenylborate, which is used as a reference compound to estimate transfer activity coefficients.<sup>[20]</sup> The voltammetric

behaviour of Keggin and Wells–Dawson-type POMs has been investigated in various solvents, and the redox potentials for the first reduction process of POMs in various organic solvents are related to their acceptor number ( $A_N$ ) and polarity ( $E_T^N$ ).<sup>[8,21–25]</sup> This relationship was recently applied to the estimation of  $A_N$  and  $E_T^N$  for a series of eight imidazolium-based RTILs.<sup>[26]</sup>

Despite several papers reporting POM electrochemistry in RTILs,<sup>[17–19,26–28]</sup> their fundamental electrochemical behaviour is still not fully investigated, especially in terms of understanding the solvation effects arising from RTILs with different chemical structures of cations and anions. RTILs have many different chemical structures, and are well known to have charged interfacial layers that are much more ordered and more dense compared with conventional salt/solvent systems.<sup>[29–31]</sup> This could affect the electrochemistry of charged analytes such as POMs (and their reduction products) because they may have different properties when interacting with these denser charged layers. It is vital to understand the detailed electrochemical behaviour of POMs in RTILs because the combination of excellent and specific chemical properties of POMs and RTILs could lead to new research areas and innovations (e.g. for use in electrochromic devices,<sup>[32]</sup> excellent catalysts<sup>[33,34]</sup> and as anticorrosion reagents).<sup>[35,36]</sup>

In this work, the electrochemical behaviour of a Wells–Dawson-type POM ( $(n-Bu_4N)_4[S_2W_{18}O_{62}]$ ) is studied using cyclic voltammetry in 12 RTILs containing a range of different anions and cations. Measurements of formal potentials and peak-to-peak separations for the different reduction processes will uncover information on the thermodynamics and kinetics of the electron transfer processes. In particular, the nature of the cation is shown to have most effect on the potentials and peak-to-peak separations, revealing solvation effects and ion-pairing of the highly negatively charged reduction products with the positively charged cations. Furthermore, two additional POMs –  $(n-Bu_4N)_6[P_2W_{18}O_{62}]$  and  $(n-Bu_4N)_3[PW_{12}O_{40}]$  – were briefly studied using the optimal RTIL for  $[S_2W_{18}O_{62}]^{4-}$  (fastest kinetics, smallest reduction potentials, symmetrical peaks and absence of impurity signals), revealing more negative potentials, but faster kinetics and asymmetric peaks, especially for  $[PW_{12}O_{40}]^{3-}$ .

## Experimental

### Chemicals and reagents

The ionic liquids 1-ethyl-3-methylimidazolium bis(trifluoromethylsulfonyl)imide ( $[\text{C}_2\text{mim}][\text{TFSI}]$ , >99.5%), 1-butyl-3-methylimidazolium bis(trifluoromethylsulfonyl)imide ( $[\text{C}_4\text{mim}][\text{TFSI}]$ , >99.5%), *N*-butyl-*N*-methylpyrrolidinium bis(trifluoromethylsulfonyl)imide ( $[\text{C}_4\text{mpyrr}][\text{TFSI}]$ , >99.5%), diethylmethylsulfonium bis(trifluoromethylsulfonyl)imide ( $[\text{S}_{2,2,1}][\text{TFSI}]$ , >99%), butyltrimethylammonium bis(trifluoromethylsulfonyl)imide ( $[\text{N}_{4,1,1,1}][\text{TFSI}]$ , >99%), octyltriethylammonium bis(trifluoromethylsulfonyl)imide ( $[\text{N}_{8,2,2,2}][\text{TFSI}]$ , >98%), methyltrioctylammonium bis(trifluoromethylsulfonyl)imide ( $[\text{N}_{1,8,8,8}][\text{TFSI}]$ , >99%), trihexyltetradecylphosphonium bis(trifluoromethylsulfonyl)imide ( $[\text{P}_{14,6,6,6}][\text{TFSI}]$ , >98%), 1-butyl-3-methylimidazolium tetrafluoroborate ( $[\text{C}_4\text{mim}][\text{BF}_4]$ , >99%), 1-butyl-3-methylimidazolium hexafluorophosphate ( $[\text{C}_4\text{mim}][\text{PF}_6]$ , >99.5%), 1-ethyl-3-methylimidazolium bis(fluorosulfonyl)imide ( $[\text{C}_2\text{mim}][\text{FSI}]$ , >98%) and 1-ethyl-3-methylimidazolium bis(pentafluoroethylsulfonyl)imide ( $[\text{C}_2\text{mim}][\text{BETI}]$ , >98%) were purchased from IoLiTec (Heilbronn, Germany) and used as received. It is noted that attempts to purify the RTILs using standard synthetic work-ups were found to have no effect on the intrinsic impurity features present in the cyclic voltammetry for some of the dried RTILs (discussed later in this work), and that cyclic voltammetry is a very sensitive technique that can be used to monitor impurities. Fig. 2 shows the chemical structures and abbreviations of the cations and anions used in this study.

A 0.5 M sulfuric acid solution was prepared by diluting sulfuric acid ( $\text{H}_2\text{SO}_4$ , 98% w/w, Merck, Kilsyth, Victoria) with ultrapure water (resistance 18.2 M $\Omega$  cm, Millipore Pty Ltd, North Ryde, NSW, Australia). Nitrogen gas was obtained from a gas line connected to a 99.99% purity  $\text{N}_2$  cylinder from the building's nitrogen supply. A 4 mM ferrocene solution was made by dissolving ferrocene (>98%, Fc,  $\text{Fe}(\text{C}_5\text{H}_5)_2$ , Sigma-Aldrich) in acetonitrile (>99.8%, Sigma-Aldrich). Acetone (>99%, Sigma-Aldrich) was used as received.

### Synthesis and characterisation of polyoxometalates

The POMs  $(n\text{-Bu}_4\text{N})_4[\text{S}_2\text{W}_{18}\text{O}_{62}]$ ,  $(n\text{-Bu}_4\text{N})_6[\text{P}_2\text{W}_{18}\text{O}_{62}]$  and  $(n\text{-Bu}_4\text{N})_3[\text{PW}_{12}\text{O}_{40}]$  were synthesised by standard literature methods.<sup>[23,37,38]</sup> All POMs were recrystallised from acetonitrile at least twice before their use in electrochemical measurements.

### Electrochemical experiments

All electrochemical experiments were performed using a PGSTAT101 Autolab potentiostat (Metrohm Autolab, Gladesville, NSW, Australia) interfaced to a PC using Nova 1.11 software, at laboratory temperature ( $295 \pm 1$  K) inside an aluminium Faraday cage to reduce electrical interference. Platinum thin-film electrodes (Pt-TFEs, ED-SE1-Pt) were purchased from MicruX Technologies (Oviedo, Spain). All Pt-TFEs have a 1-mm diameter platinum working electrode (WE), a platinum reference electrode (RE) and a platinum counter electrode (CE) built in. Electrode adapters supplied by MicruX were used to connect the Pt-TFEs to the potentiostat. All Pt-TFEs were electrochemically activated before use by drop-casting 10  $\mu\text{L}$  of 0.5 M  $\text{H}_2\text{SO}_4(\text{aq})$  onto the three electrodes and running cyclic voltammetry (CV) between  $\sim +0.7$  and  $-0.7$  V ( $\sim 100$  cycles,  $1000 \text{ mV s}^{-1}$ ) under a slow flow of nitrogen ( $\sim 100$  standard cubic centimeters per minute, sccm). The Pt-TFEs were then rinsed twice with ultrapure water followed by acetone before being dried under a stream of nitrogen.

The POM solid ( $\sim 1$  mg) was placed directly onto the WE using the tip of a small spatula, using the 'adhered solid' method.<sup>[39]</sup> Then, 5  $\mu\text{L}$  of the RTIL was dropcast to ensure that the electrodes and the POM material were fully covered with the RTIL. The electrode was then placed inside a glass T-cell, and purged with nitrogen (for  $\sim 30$  min at 500 sccm) to remove impurities that might interfere with electrochemical experiments, such as oxygen, carbon dioxide or water. CV was then carried out to determine the electrochemical reversibility of the POM  $(n\text{-Bu}_4\text{N})_4[\text{S}_2\text{W}_{18}\text{O}_{62}]$  in different RTILs, and scan rate studies were performed to determine

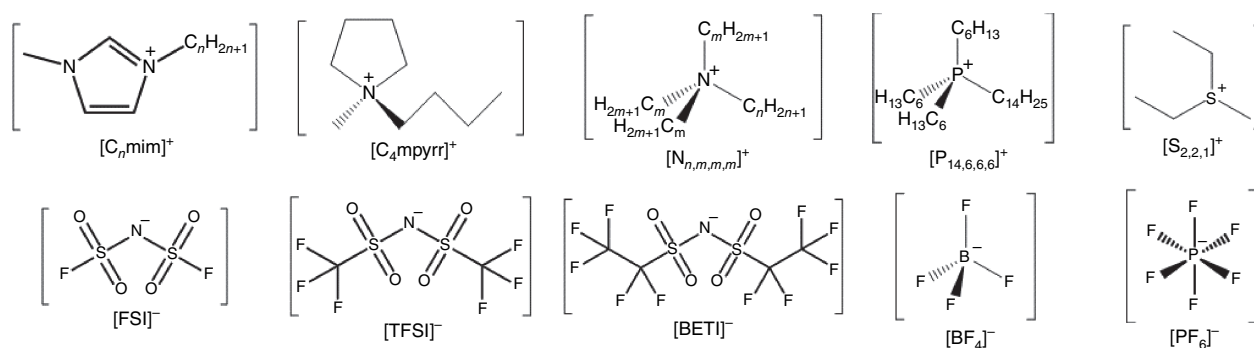


Fig. 2. Chemical structures and abbreviations of the RTIL cations and anions used in this study.

the mass transport mechanism. The two other POMs were also studied using CV in two chosen RTILs. Owing to the unstable Pt pseudo-RE present on the TFE devices, an internal standard of ferrocene ( $\sim 1 \mu\text{L}$  from a 4 mM ferrocene solution in acetonitrile) was added directly to the POM/RTIL mixture on the TFE after experiments with the POM were completed, and the acetonitrile was allowed to evaporate under nitrogen (at 500 sccm) for  $\sim 20$  min. The resulting solution of Fc and POM in the RTIL was scanned over the ferrocene/ferrocenium ( $\text{Fc}/\text{Fc}^+$ ) redox peak and the full reductive window of the POM to determine the reduction potentials of the POMs vs  $\text{Fc}/\text{Fc}^+$ .

Blank scans (RTIL without the POM) were obtained by dropcasting the RTIL of choice ( $\sim 5 \mu\text{L}$ ) onto the Pt-TFE such that all the electrodes were fully covered. The electrode was then placed into a glass T-cell and purged under nitrogen (at 500 sccm for  $\sim 30$  min) to remove atmospheric impurities and CV was recorded for the blank RTIL at a scan rate of  $100 \text{ mV s}^{-1}$ . As RTILs are known to contain intrinsic impurities that are often redox-active in the potential window,<sup>[40]</sup> recording the blank CV was important to determine which redox peaks were arising directly from the POM, and which were from the RTILs. All experiments were performed under a high flow of dried nitrogen (relative humidity level of  $< 1\%$ ), which is sufficient to remove voltammetric peaks arising from dissolved oxygen and water.<sup>[40]</sup> Although there may still be some water present even in the 'dried' RTILs (e.g.  $\sim$ tens to hundreds of parts per million), there is no evidence of water-induced oxidation or reduction signals in the cyclic voltammograms of the blank RTILs. This observation is important, especially for platinum electrodes, which are known to be more sensitive to water and oxide formation<sup>[41]</sup> compared with more inert surfaces such as glassy carbon.

## Results and discussion

### Adhesion of solid POM to the electrode surface

To study the effect of the RTIL cation and anion structures on POM electrochemistry (kinetics and thermodynamics), the POM  $(n\text{-Bu}_4\text{N})_4[\text{S}_2\text{W}_{18}\text{O}_{62}]$  was first investigated in 12 different RTILs containing a range of different cations and anions (see Fig. 2). Because POMs are known to have limited solubility in RTILs,<sup>[26,28]</sup> attempts to dissolve low millimolar concentrations were first made; however, full dissolution was visually observed only in 6 of the 12 RTILs (see supplementary information for details). Therefore, the 'adhered solid' method reported by Zhang and Bond<sup>[39]</sup> was utilised for the present study in all RTILs for consistency and to enable comparison of the behaviour in all RTILs. This method shows apparent equivalent voltammetry (except for the current magnitude) for species that are dissolved in solution vs adhered to the electrode,<sup>[39]</sup> which we also

observed for the POMs in this work. Therefore, by attaching solid POM to the electrode, peak potentials and peak-to-peak separations could be more accurately analysed and compared, while also giving sufficient currents to overcome the limited solubility of the POM in some of the RTILs.

### Electrochemical reduction of $(n\text{-Bu}_4\text{N})_4[\text{S}_2\text{W}_{18}\text{O}_{62}]$ in different ionic liquids

Cyclic voltammetry for the electrochemical reduction of the adhered POM  $(n\text{-Bu}_4\text{N})_4[\text{S}_2\text{W}_{18}\text{O}_{62}]$  was carried out in all 12 RTILs under dry nitrogen over the entire available potential window before the breakdown of the RTIL solvent. In all RTILs, the first two reduction peaks were clearly defined and showed chemically reversible peak shapes. The CVs are presented in Fig. 3; the green curve shows the scans reversed after the first peak, and the red curve shows the scans reversed after the second peak. It can be seen that both electron transfer processes appear to be chemically reversible owing to the presence of an oxidative back-peak after the reduction, with peak shapes relatively symmetric for the forward vs reverse currents, as observed previously for the same POM in RTIL solvents.<sup>[17,26]</sup> It is important to note that some of the ILs contained intrinsic impurities that showed redox activity in the reductive potential region, making observation of the additional POM reduction processes after the second reduction peak difficult. This was particularly problematic in the ammonium-based RTILs, where large impurity peaks were consistently observed, noting that the additional oxidation peak that can be seen at  $\sim 0.2 \text{ V}$  vs Pt in the  $[\text{N}_{1,8,8,8}][\text{TFSI}]$  RTIL (Fig. 3I) is also present in the blank scan, and was assigned to an impurity. Although all RTILs were purchased from commercial suppliers at the highest purities possible, they often contain intrinsic impurities that are redox active.<sup>[40]</sup> Usually, these impurity peaks are much smaller than the analyte signals,<sup>[40]</sup> but because of the low solubility of the POM in RTILs, the POM redox peak currents themselves are very small, and appear similar in size to the impurity peaks. These impurities cannot be easily removed, meaning that they can interfere with measuring the redox process of interest. This was also discussed previously by Zhang *et al.* in their study of POM reduction in the RTIL  $[\text{C}_4\text{mim}][\text{BF}_4]$ .<sup>[17]</sup>

In six of the RTILs, additional redox processes up to a total of five or six peaks were observed (see Fig. 4, labelled in roman numerals) before the edge of the electrochemical window. In the RTILs  $[\text{C}_2\text{mim}][\text{FSI}]$ ,  $[\text{C}_2\text{mim}][\text{TFSI}]$ ,  $[\text{C}_4\text{mim}][\text{TFSI}]$ ,  $[\text{C}_4\text{mpyrr}][\text{TFSI}]$  and  $[\text{C}_4\text{mim}][\text{PF}_6]$ , a total of six reduction peaks were observed, and five reduction peaks were observed in the RTIL  $[\text{P}_{14,6,6,6}][\text{TFSI}]$ . It is noted that in  $[\text{C}_2\text{mim}][\text{TFSI}]$ ,  $[\text{C}_4\text{mim}][\text{TFSI}]$  and  $[\text{C}_4\text{mim}][\text{PF}_6]$ , a slightly larger peak current for peak IV was observed at  $\sim -1.1 \text{ V}$  vs Pt, which is most likely due to the overlap from small impurity signals that were present in the blank; this does not affect the measurement of the peak potentials

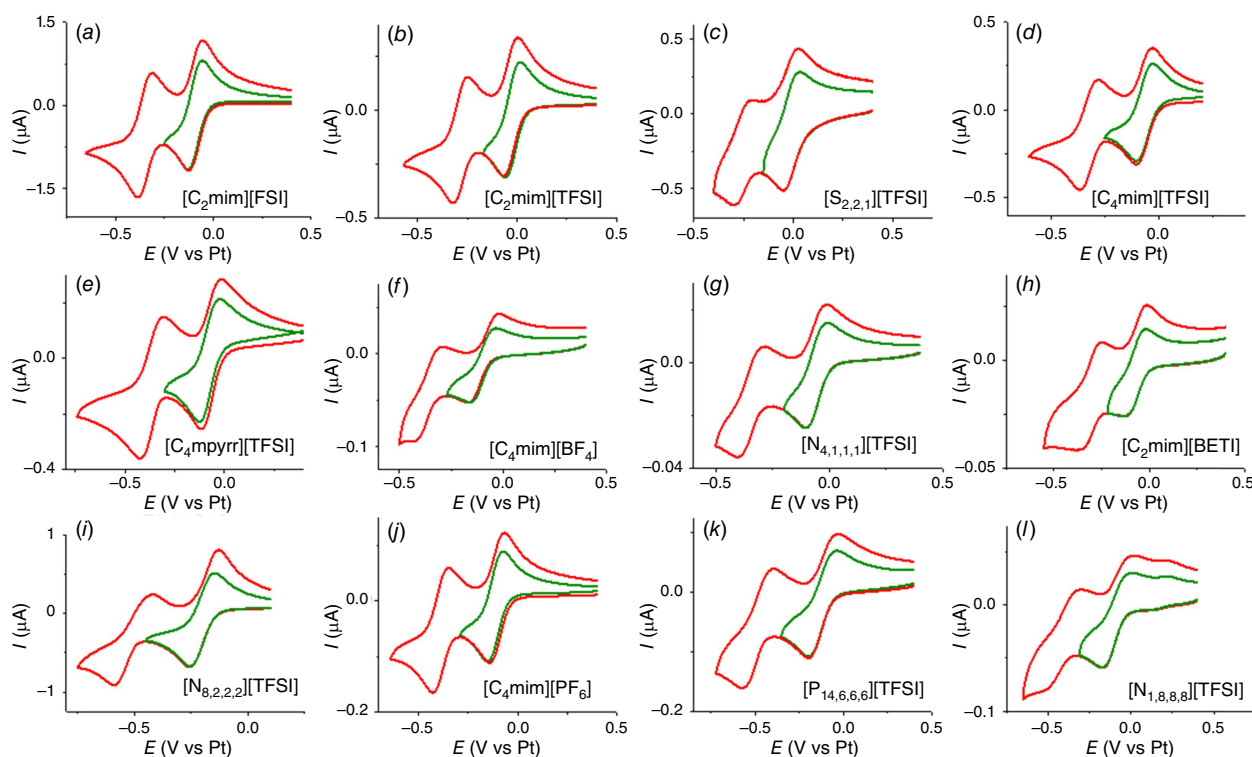


**Fig. 3.** Cyclic voltammograms for the first two reduction processes of  $(n\text{-Bu}_4\text{N})_6[\text{S}_2\text{W}_{18}\text{O}_{62}]$  in (a)  $[\text{C}_2\text{mim}][\text{FSI}]$ ; (b)  $[\text{C}_2\text{mim}][\text{TFSI}]$ ; (c)  $[\text{S}_{2,2,1}][\text{TFSI}]$ ; (d)  $[\text{C}_4\text{mim}][\text{TFSI}]$ ; (e)  $[\text{C}_4\text{mpyrr}][\text{TFSI}]$ ; (f)  $[\text{C}_4\text{mim}][\text{BF}_4]$ ; (g)  $[\text{N}_{4,1,1,1}][\text{TFSI}]$ ; (h)  $[\text{C}_2\text{mim}][\text{BETI}]$ ; (i)  $[\text{N}_{8,2,2,2}][\text{TFSI}]$ ; (j)  $[\text{C}_4\text{mim}][\text{PF}_6]$ ; (k)  $[\text{P}_{14,6,6,6}][\text{TFSI}]$ ; and (l)  $[\text{N}_{1,8,8,8}][\text{TFSI}]$  on a Pt TFE ( $d = 1 \text{ mm}$ ) at a scan rate of  $100 \text{ mV s}^{-1}$ .

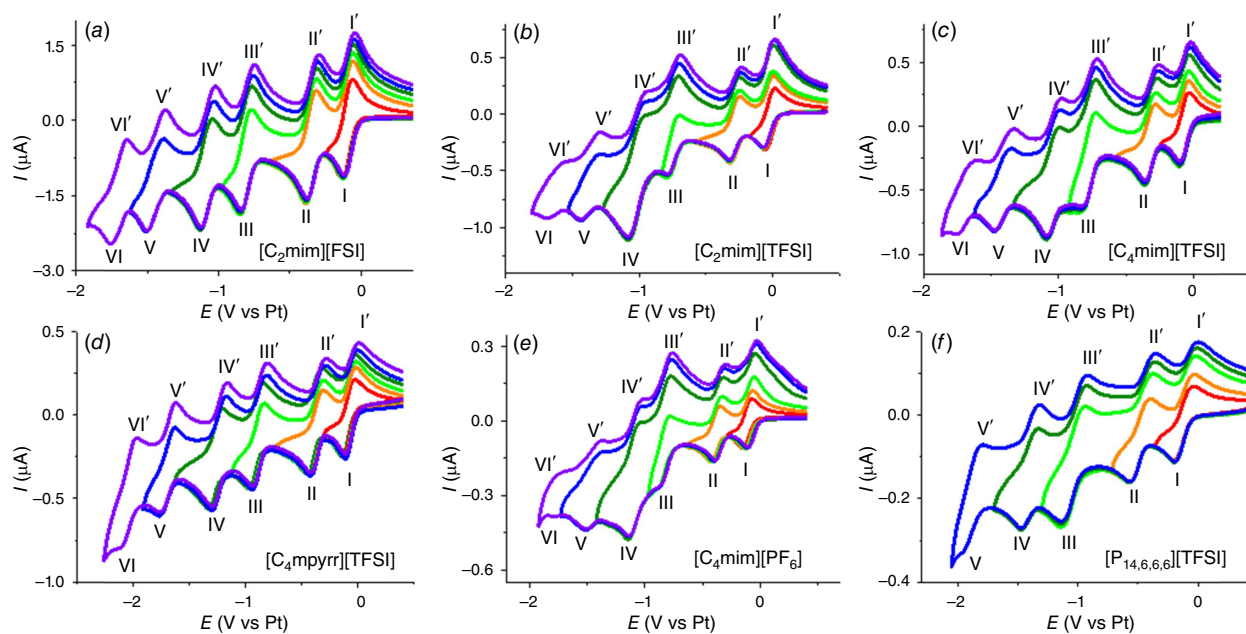


**Fig. 4.** Cyclic voltammograms for six reduction processes of  $(n\text{-Bu}_4\text{N})_4[\text{S}_2\text{W}_{18}\text{O}_{62}]$  in (a)  $[\text{C}_2\text{mim}][\text{FSI}]$ ; (b)  $[\text{C}_2\text{mim}][\text{TFSI}]$ ; (c)  $[\text{C}_4\text{mim}][\text{TFSI}]$ ; (d)  $[\text{C}_4\text{mpyrr}][\text{TFSI}]$ ; (e)  $[\text{C}_4\text{mim}][\text{PF}_6]$ ; and (f)  $[\text{P}_{14,6,6,6}][\text{TFSI}]$  on a Pt TFE ( $d = 1 \text{ mm}$ ) at a scan rate of  $100 \text{ mV s}^{-1}$ .

and separations for the analysis. Fig. 4 also includes CV scans where the potential is reversed after each reduction peak, to show the reversibility of each process. Generally, the imidazolium and pyrrolidinium cation-based RTILs showed clear reversible reduction peaks. The two RTILs that showed the most 'symmetrical' processes for  $[S_2W_{18}O_{62}]^{4-}$ , and were least affected by impurities, were  $[C_2mim][FSI]$  and  $[C_4mpyrr][TFSI]$ .  $[C_2mim][FSI]$  is notably the least viscous RTIL, with a viscosity of  $\sim 19$  cP,<sup>[42]</sup> whereas the RTIL  $[C_4mpyrr][TFSI]$  also has a relatively low viscosity (78 cP)<sup>[43]</sup> compared with most of the other RTILs in this study.

To determine the mass transport behaviour, scan rate studies were carried out between 10 and 1000  $mV s^{-1}$  and the peak current for the first reduction peak was measured at all scan rates in the 12 RTILs (see Supplementary Tables S1–S8, Supplementary Figs S1–S3 for data in all RTILs). Plots of peak I current vs the square root of the scan rate (see Supplementary Fig. S4), according to the Randles–Sevcik equation,<sup>[44,45]</sup> were linear for all RTILs, suggesting that the POM undergoes diffusion-controlled mass transport, even though the solid was physically adhered to the surface of the working electrode. This is consistent with the observations made previously by Zhang and Bond,<sup>[39]</sup> supporting the method as suitable for studying the reduction potentials and kinetics of electron transfer processes.

An understanding of the redox kinetics for an electron transfer process can be inferred from measuring the peak-to-peak separation ( $\Delta E_p$ ), which is calculated from the potential difference between the reduction and oxidation peak

potentials,  $|E_p^{red} - E_p^{ox}|$ . In conventional solvent/electrolyte systems, an ideal fast reversible one-electron redox process has a  $\Delta E_p$  close to 59 mV (Butler–Volmer equation),<sup>[45]</sup> but this value is known to be highly dependent on various factors, including the nature of the electrode surface (e.g. Pt, Au, glassy carbon), oxide formation, temperature, uncompensated resistance (iR drop) and inner-sphere vs outer-sphere reaction mechanism. In RTILs,  $\Delta E_p$  for an 'ideal' redox couple,  $Fc/Fc^+$ , is usually larger than 59 mV, and has been reported to increase with scan rate and concentration.<sup>[46]</sup> For example, on a Pt TFE,  $\Delta E_p$  for  $Fc/Fc^+$  (3 mM concentration of Fc) in RTILs is between 78 and 98 mV in the 12 RTILs at 100  $mV s^{-1}$  (third column in Table 1), and does not appear to depend on solvent viscosity, despite an order of magnitude difference in the diffusion coefficient of Fc from the least to the most viscous RTIL.<sup>[47]</sup>

Table 1 also shows the  $\Delta E_p$  for all the visible POM reduction peaks shown in Figs 3, 4 on a Pt TFE. The peak-to-peak separation data for the POMs (peak I/I', 76–198 mV) are found to be much more variable than for  $Fc/Fc^+$  as the RTIL structure is changed, suggesting some dependence on solvation, which is more than just a viscosity/diffusion coefficient effect. The smallest peak-to-peak separation (i.e. the fastest kinetics) for the first reduction process (labelled I/I') is observed in the RTILs  $[C_2mim][FSI]$  and  $[S_{2,2,1}][TFSI]$ . Although these are two of the least viscous RTILs, there does not appear to be a systematic trend in the peak-to-peak separations with increasing viscosity, as shown in Table 1. However, comparing  $[C_2mim]^+$  RTILs, when

**Table 1.** Peak-to-peak separations ( $\Delta E_p$ ) for the ferrocene/ferrocenium ( $Fc/Fc^+$ ) redox couple, and the redox processes of the POM  $[S_2W_{18}O_{62}]^{4-}$  on a Pt-TFE in 12 RTILs.

Ionic liquid	Viscosity $\eta^A$ (cP)	$\Delta E_p$ for $Fc/Fc^+$ (mV)	$\Delta E_p$ , for $[S_2W_{18}O_{62}]^{4-}$ (mV) at 100 $mV s^{-1}$					
		at 100 $mV s^{-1}$ (ref. [48] and present work)	I/I'	II/II'	III/III'	IV/IV'	V/V'	VI/VI'
$[C_2mim][FSI]$	22 <sup>[42]</sup>	81	76	85	93	100	127	125
$[C_2mim][TFSI]$	34 <sup>[47]</sup>	98	90	90	100	137	137	112
$[S_{2,2,1}][TFSI]$	50 <sup>[47]</sup>	91	76	98	(117)	(134)	–	–
$[C_4mim][TFSI]$	52 <sup>[47]</sup>	94	78	100	115	110	132	149
$[C_4mpyrr][TFSI]$	89 <sup>[47]</sup>	84	120	139	134	132	147	164
$[C_4mim][BF_4]$	112 <sup>[47]</sup>	86	156	142	–	–	–	–
$[N_{4,1,1,1}][TFSI]$	138 <sup>[47]</sup>	78	93	117	(142)	(98)	n/a	(76)
$[C_2mim][BETI]$	153 <sup>[49]</sup>	86	127	134	–	–	–	–
$[N_{8,2,2,2}][TFSI]$	288 <sup>[50]</sup>	90	129	173	–	–	–	–
$[C_4mim][PF_6]$	371 <sup>[47]</sup>	91	81	93	134	127	112	n/a
$[P_{14,6,6,6}][TFSI]$	450 <sup>[47]</sup>	91	198	215	222	151	147	–
$[N_{1,8,8,8}][TFSI]$	676 <sup>[51]</sup>	97	190	225	–	–	–	–

–, value was either not measured or a peak was not clearly visible for these processes.

(number), peaks overlaid impurity signals, but could still be measured.

n/a, peak was visible, but the value was difficult to measure because of the broad nature of the peak or presence of impurity.

<sup>A</sup>Dynamic viscosity measured at  $\sim 293$  K and standard pressure ( $\sim 1$  atm).

increasing the chain length and the number of fluorinated groups on both sides of the bis(sulfonylimide) by varying the anion from  $[\text{FSI}]^-$  to  $[\text{TFSI}]^-$  to  $[\text{BETI}]^-$ ,  $\Delta E_p$  increases for the first two redox couples. Another trend is observed for the ammonium-based RTILs with a common  $[\text{TFSI}]^-$  anion, where the addition of alkyl groups from  $[\text{N}_{4,1,1,1}]^+$  to  $[\text{N}_{8,2,2,2}]^+$  to  $[\text{N}_{1,8,8,8}]^+$  increases the bulkiness of the cation and viscosity of the RTIL, resulting in an increase in  $\Delta E_p$ . It is also possible that the longer fatty chains (which also shield the cationic charge) improve preferential adhesion onto the WE surface, which could in turn increase ohmic drop and result in a larger  $\Delta E_p$ .

Fig. 5 shows a plot of the  $\Delta E_p$  values for successive redox couples in the six RTILs where multiple peaks were observed. Consistent with previous literature,<sup>[25]</sup> a general trend of progressively increasing  $\Delta E_p$  is observed in most RTILs as the reduction proceeds. The exception is the RTIL  $[\text{P}_{14,6,6,6}][\text{TFSI}]$ , where a wide  $\Delta E_p$  close to  $\sim 200$  mV was observed for the first three redox processes, which then decreased to  $\sim 150$  mV for the fourth and fifth reduction. Unusual behaviour for the same cation has been documented multiple times previously,<sup>[47,52,53]</sup> and is thought to be related to its structure, which has a central positive charge surrounded by long and flexible carbon chains. This makes the solvation of negatively charged analyte species much more difficult owing to steric hindrance at the charged centre, resulting in slower kinetics compared with the more freely accessible charges on the imidazolium and pyrrolidinium cations. Comparing the different cation structures, the general trend observed in  $\Delta E_p$  for the first reduction process is: imidazolium < pyrrolidinium < phosphonium, the same as was observed for 2,4,6-trinitrotoluene reduction.<sup>[48]</sup> This suggests that cation solvation effects play an important role in the reduction of negatively charged

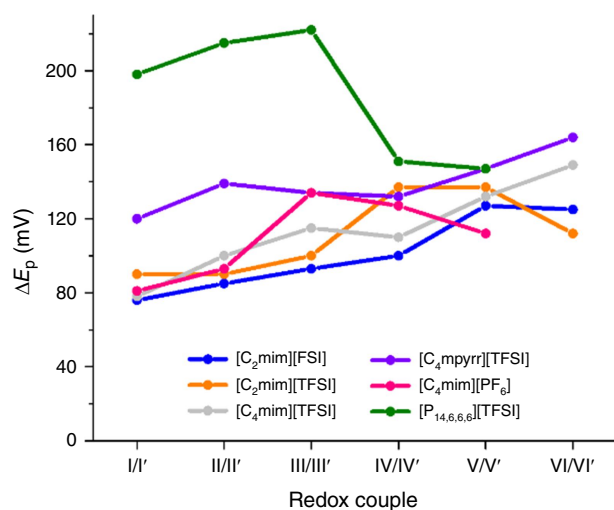


**Fig. 5.** Plot of peak-to-peak separations ( $\Delta E_p$ ) for the six redox processes of  $[\text{S}_2\text{W}_{18}\text{O}_{62}]^{4-}$  in six different RTILs at a scan rate of  $100 \text{ mV s}^{-1}$ .

species such as POMs. To compare with a conventional solvent/salt system,  $\Delta E_p$  for the first two processes of  $(n\text{-Bu}_4\text{N})_4[\text{S}_2\text{W}_{18}\text{O}_{62}]$  on a Pt electrode in acetonitrile (+ 0.5 M  $[n\text{-Bu}_4\text{N}][\text{PF}_6]$  supporting electrolyte) was reported to be 68 and 90 mV for I/I' and II/II', respectively,<sup>[25]</sup> which is similar to some of the less viscous RTILs in the present study. The other peaks in acetonitrile were reported to be poorly defined on a Pt electrode, or overlapping with the solvent reduction process,<sup>[25]</sup> demonstrating the clear advantage of using RTILs for observing the multiple reduction processes at more accessible potentials.

In order to assess the thermodynamics of the reduction processes, the mid-point potentials,  $E_{\text{mid}} = (E_p^{\text{red}} - E_p^{\text{ox}})/2$ , were measured for all visible peaks in the 12 RTILs, as shown in Table 2. Mid-point potentials (rather than reduction peak potentials) for the POM transitions were used to assess the thermodynamics without the effect of the different heterogeneous electron transfer kinetics in the RTILs. Ferrocene was added *in situ* to the POM/RTIL solution, and the potentials were shifted so that the midpoint of the  $\text{Fc}/\text{Fc}^+$  redox couple was at 0 V. Ferrocene is commonly used as a reference potential scale in RTIL solvents.<sup>[54,55]</sup>

The  $E_{\text{mid}}$  values reported in Table 2 compare very well with other previously reported reduction potentials for similar POMs in RTILs,<sup>[17,26]</sup> noting that these experiments were performed on different electrodes, so some variation is expected. Interestingly, the  $E_{\text{mid}}$  values in the 12 RTILs are  $\sim 200$  mV less negative than previously reported in a conventional solvent system (acetonitrile + 0.5 M  $[n\text{-Bu}_4\text{N}][\text{PF}_6]$ ), which were  $-0.233$  and  $-0.606$  V vs  $\text{Fc}/\text{Fc}^+$  for I/I' and II/II', respectively.<sup>[25]</sup> The difference in reduction potential was assigned to the different polarity of the solvents by Rahman *et al.*,<sup>[25]</sup> with the most negative  $E_{\text{mid}}$  values observed in the least polar solvent studied, dichloromethane, and the least negative  $E_{\text{mid}}$  observed in the most polar solvent, water. The  $E_{\text{mid}}$  values observed in RTILs both in our study and in a previous study by Zhang *et al.*<sup>[17]</sup> are comparable with those in water. However, the much wider available potential windows of RTILs compared with water allow the observation of the multiple reduction processes, again supporting the use of RTILs as favourable solvents for observing POM reduction processes.

The mid-point potentials in the 12 RTILs range from +67 to  $-34$  mV, but there appears to be no clear trend with increasing viscosity or with cation or anion structure. However, the trends become more visually clear when all six reduction processes are plotted together (see Fig. 6). Whereas the first reduction process (I/I') at potentials close to zero has  $\sim 100$  mV variation, by the fifth and sixth reduction processes, these differences are as high as  $\sim 500$  mV (cf.  $[\text{C}_2\text{mim}]^+$  cation vs  $[\text{P}_{14,6,6,6}]^+$  cation for V/V'). In fact, the reduction potential for the VI/VI' process in  $[\text{P}_{14,6,6,6}][\text{TFSI}]$  is so significantly more negative that it is out of the range of the available potential window, explaining why only five processes are observed in this RTIL. Fig. 6 therefore

**Table 2.** Reduction mid-point potentials ( $E_{\text{mid}}$ ) for the POM  $[\text{S}_2\text{W}_{18}\text{O}_{62}]^{4-}$  in different RTILs on a Pt electrode.

Ionic liquid	Viscosity $\eta^{\text{A}}$ (cP)	$E_{\text{mid}}$ (mV) for $[\text{S}_2\text{W}_{18}\text{O}_{62}]^{4-}$ vs Fc/Fc <sup>+</sup> (mV) at 100 mV s <sup>-1</sup>					
		I/I'	II/II'	III/III'	IV/IV'	V/V'	VI/VI'
[C <sub>2</sub> mim][FSI]	22 <sup>[42]</sup>	44	-211	-671	-950	-1315	-1573
[C <sub>2</sub> mim][TFSI]	34 <sup>[47]</sup>	43	-209	-670	-945	-1297	-1560
[S <sub>2,2,1</sub> ][TFSI]	50 <sup>[47]</sup>	-34	-273	(-751)	(-1099)	-	-
[C <sub>4</sub> mim][TFSI]	52 <sup>[47]</sup>	-1	-249	-713	-974	-1354	-1629
[C <sub>4</sub> mpyrr][TFSI]	89 <sup>[47]</sup>	44	-254	-777	-1136	-1601	-1963
[C <sub>4</sub> mim][BF <sub>4</sub> ]	112 <sup>[47]</sup>	22	-254	-	-	-	-
[N <sub>4,1,1,1</sub> ][TFSI]	138 <sup>[56]</sup>	40	-243	(-737)	(-1033)	n/a	(-1832)
[C <sub>2</sub> mim][BETI]	153 <sup>[49]</sup>	-26	-264	-	-	-	-
[N <sub>8,2,2,2</sub> ][TFSI]	288 <sup>[50]</sup>	-26	-348	-	-	-	-
[C <sub>4</sub> mim][PF <sub>6</sub> ]	371 <sup>[47]</sup>	43	-237	-709	-967	-1341	-1646
[P <sub>14,6,6,6</sub> ][TFSI]	450 <sup>[47]</sup>	-21	-386	-951	-1324	-1817	-
[N <sub>1,8,8,8</sub> ][TFSI]	676 <sup>[51]</sup>	67	-323	-	-	-	-

Note: potentials were accurate to  $\sim\pm 2$  mV on repeat experiments.

(number), peaks overlaid impurity signals, but could still be measured.

n/a, peak was visible, but the value was difficult to measure because of the overlap with impurity peak.

<sup>A</sup>Dynamic viscosity measured at  $\sim 293$  K and standard pressure ( $\sim 1$  atm).

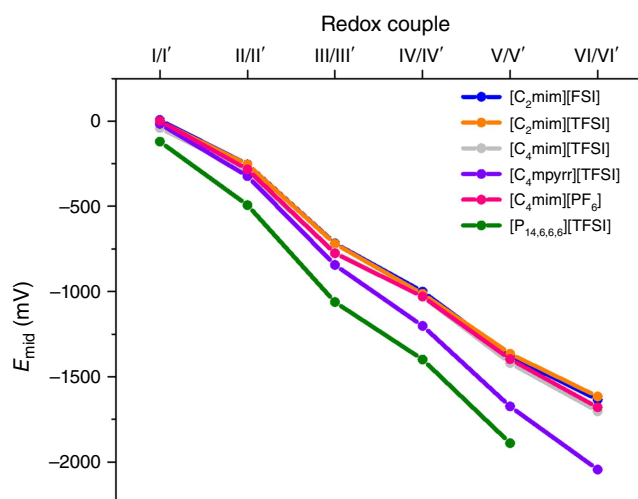


**Fig. 6.** Plot of mid-point potentials ( $E_{\text{mid}}$ ) for the six redox processes of  $[\text{S}_2\text{W}_{18}\text{O}_{62}]^{4-}$  in the six RTILs that showed multiple successive peaks.

clearly shows that the differences in cation solvation are much more evident as the POM becomes more negatively charged.  $E_{\text{mid}}$  data for the  $[\text{S}_{2,2,1}]^+$  and  $[\text{N}_{4,1,1,1}]^+$  cations have also been included in Table 2 in parentheses, but these peaks had some overlap with impurity signals (see CV scans in the Supplementary Fig. S5). However, these data provide important information showing that the trend in voltage response with respect to cation structure follows  $[\text{C}_2\text{mim}]^+ < [\text{C}_4\text{mim}]^+ < [\text{S}_{2,2,1}]^+ \approx [\text{N}_{4,1,1,1}]^+ < [\text{C}_4\text{mpyrr}]^+ < [\text{P}_{14,6,6,6}]^+$ , with imidazolium RTILs clearly the best choice for observation of higher-order reduction processes at lower potentials.

Because of the low solubility of the POM in the RTILs, it was not possible to accurately calculate diffusion coefficients using the Shoup and Szabo<sup>[57]</sup> method. However, diffusion coefficients have been previously estimated for POMs in RTILs, and are typically very small, e.g.  $\sim 0.6 \times 10^{-8} \text{ cm}^2 \text{ s}^{-1}$  in  $[\text{C}_4\text{mim}][\text{PF}_6]$ ,<sup>[18]</sup> close to the self-diffusion coefficients of the ions of the RTIL.<sup>[58]</sup> The ratio of the diffusion coefficient of the oxidised and reduced species can affect the mid-point potential according to the following equation:<sup>[59]</sup>

$$E_{\text{mid}} = E_0 + \frac{RT}{2F} \ln\left(\frac{D_{\text{B}}}{D_{\text{A}}}\right) \quad (1)$$

where  $E_0$  is the formal potential,  $R$  is the universal gas constant,  $T$  is the temperature,  $F$  is Faraday's constant and  $D_{\text{B}}$  and  $D_{\text{A}}$  are the diffusion coefficients of the reduced and oxidised POM species, respectively. It is usually assumed that  $D_{\text{B}}$  and  $D_{\text{A}}$  are equal,<sup>[59,60]</sup> but a  $\sim 30\times$  difference was observed between the oxygen/superoxide ( $\text{O}_2/\text{O}_2^{\cdot-}$ ) redox couple in an ammonium cation-based RTIL.<sup>[61]</sup> Such a large variation, however, is not expected for the POM and its reduction product, because of the more similar surface charge densities of  $[\text{S}_2\text{W}_{18}\text{O}_{62}]^{4-}/[\text{S}_2\text{W}_{18}\text{O}_{62}]^{5-}$  compared with  $\text{O}_2/\text{O}_2^{\cdot-}$ . However, we performed a simulation with DigiSim using a  $10\times$  difference in diffusion coefficient, and observed only a  $\sim 30$  mV shift in  $E_{\text{mid}}$ . This gives us confidence that the much larger shifts in  $E_{\text{mid}}$  between the different RTILs (Fig. 6) mostly arise from different solvation effects from the RTIL cations, even if the ratio of  $D_{\text{A}}$  and  $D_{\text{B}}$  varies in some of the RTILs.

## Electrochemical studies of the POMs (*n*-Bu<sub>4</sub>N)<sub>6</sub>[P<sub>2</sub>W<sub>18</sub>O<sub>62</sub>] and (*n*-Bu<sub>4</sub>N)<sub>3</sub>[PW<sub>12</sub>O<sub>40</sub>] in [C<sub>2</sub>mim][FSI]

To gain further knowledge on the electron transfer of POMs in ionic liquids, two other phosphorus-based POMs were studied in the most optimal RTIL (fastest kinetics and lowest reduction potentials) found from the first POM, which was [C<sub>2</sub>mim][FSI]. The POMs studied were the phosphorous Wells–Dawson-type (*n*-Bu<sub>4</sub>N)<sub>6</sub>[P<sub>2</sub>W<sub>18</sub>O<sub>62</sub>], and the Keggin-type (*n*-Bu<sub>4</sub>N)<sub>3</sub>[PW<sub>12</sub>O<sub>40</sub>] POM. As seen in Fig. 7, CVs for [P<sub>2</sub>W<sub>18</sub>O<sub>62</sub>]<sup>6-</sup> reduction showed a total of six peaks, whereas [PW<sub>12</sub>O<sub>40</sub>]<sup>3-</sup> gave only four reduction peaks. A plot of peak current vs the square root of scan rate for the first reduction peak of [P<sub>2</sub>W<sub>18</sub>O<sub>62</sub>]<sup>6-</sup> was linear (see Supplementary Fig. S6), suggesting diffusion-controlled behaviour for the first process. However, this plot was slightly curved for the Keggin-type [PW<sub>12</sub>O<sub>40</sub>]<sup>3-</sup> POM (Supplementary Fig. S7), suggesting that more complicated mass transport mechanisms are occurring.

For this POM, there was also noticeable asymmetry seen in the reduction/oxidation peaks. Behaviour similar to this for oxygen reduction was previously reported on microdisk electrodes, where the voltammetry displayed both steady-state and transient wave shapes on the same scan, which was assigned to dramatically different diffusion coefficients (a factor of 30) for the two species (oxygen/superoxide) involved in the redox couple.<sup>[61]</sup> However, attempts to simulate the POM voltammetry using the digital simulation program DigiSim on the macrodisk-sized electrodes

(1-mm diameter) did not yield the same-shaped peaks, even with two orders of magnitude difference in diffusion coefficient (*D*), suggesting that the discrepancy in *D* is not the reason for this unusual shape. Attempts were also made to vary other parameters in the DigiSim program, such as concentration, transfer coefficient, scan rate and electron transfer rate constant, but none of these gave the desired asymmetric peak shape. However, changing the boundary conditions from ORB (open to the bulk solution) to BRB (blocked from interacting with the bulk solution) resulted in similar shaped voltammetry (see Supplementary Fig. S8 for more details). This could imply that this POM exhibits some degree of adsorption behaviour, which is not unexpected because the material is physically attached to the electrode, and this is consistent with the scan rate studies. Additionally, because of the much denser ion structuring at the RTIL/electrode interface, there may be some ‘adsorption’ into the interfacial charge layers, which could slow the movement of the electrogenerated product and produce the asymmetric peak shape. The Keggin-type POM was noticeably less soluble than the other two Wells–Dawson POMs in this RTIL, suggesting that it would preferentially remain adsorbed on the electrode surface (or near the interfacial layers), rather than dissolve into the solvent. This observation warrants further investigations in follow-up studies for this POM, but is out of the scope of the current work.

Table 3 shows the peak-to-peak separations ( $\Delta E_p$ ) and the mid-point potentials ( $E_{mid}$ ) for the six reduction processes

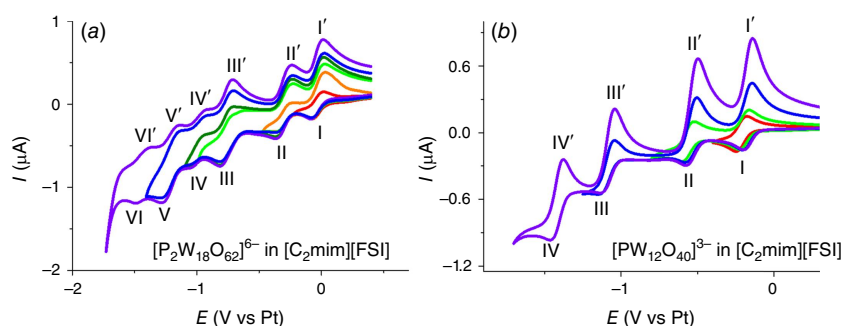


**Fig. 7.** Cyclic voltammograms for the reductions of the POM (a) (*n*-Bu<sub>4</sub>N)<sub>6</sub>[P<sub>2</sub>W<sub>18</sub>O<sub>62</sub>], and (b) (*n*-Bu<sub>4</sub>N)<sub>3</sub>[PW<sub>12</sub>O<sub>40</sub>] in [C<sub>2</sub>mim][FSI] at 100 mV s<sup>-1</sup>.

**Table 3.** Peak-to-peak separations ( $\Delta E_p$ ) and midpoint potentials ( $E_{mid}$ ) for the redox peaks of the POMs [P<sub>2</sub>W<sub>18</sub>O<sub>62</sub>]<sup>6-</sup> and [PW<sub>12</sub>O<sub>40</sub>]<sup>3-</sup> in the RTIL [C<sub>2</sub>mim][FSI] at 100 mV s<sup>-1</sup>.

	Peak	[P <sub>2</sub> W <sub>18</sub> O <sub>62</sub> ] <sup>6-</sup>		[PW <sub>12</sub> O <sub>40</sub> ] <sup>3-</sup>	
		$\Delta E_p$ (mV)	$E_{mid}$ vs Fc/Fc <sup>+</sup> (mV)	$\Delta E_p$ (mV)	$E_{mid}$ vs Fc/Fc <sup>+</sup> (mV)
[C <sub>2</sub> mim][FSI]	I/I'	98	-421	63	-372
	II/II'	109	-684	81	-731
	III/III'	103	-1154	81	-1272
	IV/IV'	110	-1399	83	-1605
	V/V'	105	-1546	–	–
	VI/VI'	81	-1814	–	–

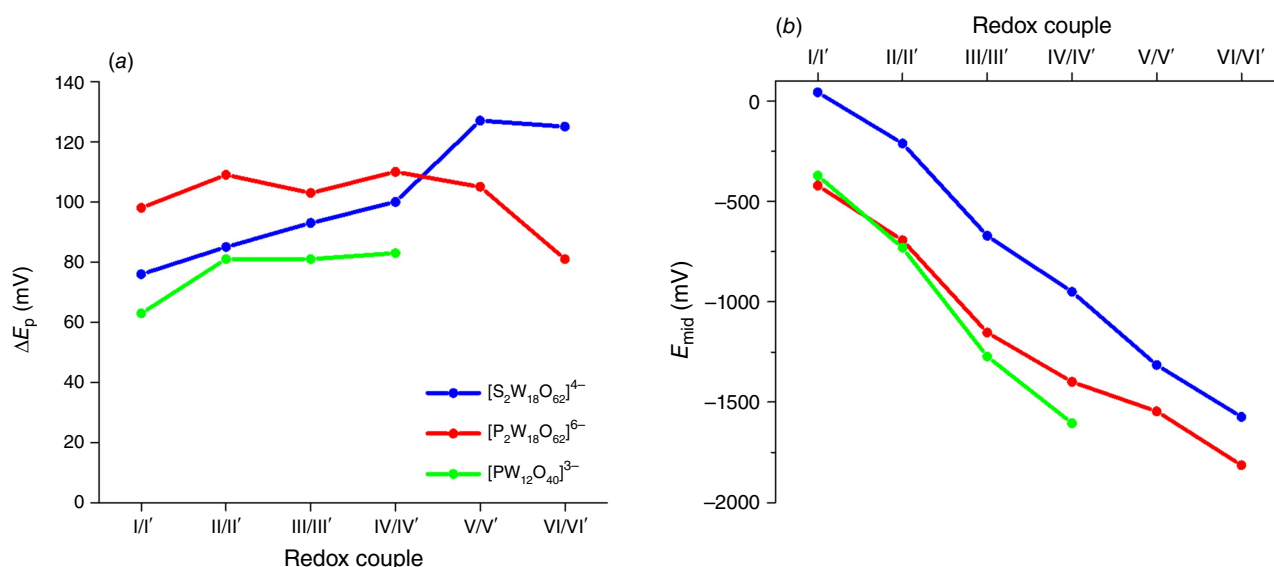


**Fig. 8.** Plot of (a) peak-to-peak separations ( $\Delta E_p$ ), and (b) mid-point potentials ( $E_{mid}$ ) for the redox peaks of the three different POMs in the RTIL  $[C_2mim][FSI]$  at a scan rate of  $100 \text{ mV s}^{-1}$ .

of  $[P_2W_{18}O_{62}]^{6-}$  and the four reduction processes of  $[PW_{12}O_{40}]^{3-}$ .  $\Delta E_p$  was slightly variable between the POMs, with the Keggin-type POM exhibiting faster kinetics for the electron transfer process. However, the  $E_{mid}$  potentials were significantly more negative for the phosphorus POMs, indicating that the successive reduction processes were more thermodynamically difficult. These values are plotted in Fig. 8 to visually show the differences. In Fig. 8a,  $\Delta E_p$  increases or remains steady on successive electron additions for the phosphorus POMs. Overall, they all exhibit relatively fast kinetics in this IL in relation to other species in RTILs.

$E_{mid}$  for  $[P_2W_{18}O_{62}]^{6-}$  vs  $[S_2W_{18}O_{62}]^{4-}$  is  $\sim 450 \text{ mV}$  different for the first reduction process (I/I'), but this difference decreases to  $\sim 240 \text{ mV}$  for peak VI/VI' (Fig. 8b), suggesting better solvation of the more negatively charged phosphorus species (up to 10 negative charges) as the reduction proceeds. Interestingly, the reduction potentials for the Keggin-type  $[PW_{12}O_{40}]^{3-}$  are  $\sim 400 \text{ mV}$  more negative compared with  $[S_2W_{18}O_{62}]^{4-}$ , even though the charges on the species are similar (3- vs 4-). The progression of the reduction potentials follows a similar trend for the two POMs and explains why only four peaks were observed in  $[PW_{12}O_{40}]^{3-}$  because the edge of the potential window in the RTIL was already reached after the fourth reduction in  $[PW_{12}O_{40}]^{3-}$ . It is noted that the potentials are similar to those reported by other researchers for the same POM compounds in RTILs.<sup>[19,27,28]</sup>

## Conclusions

The reduction of the  $[S_2W_{18}O_{62}]^{4-}$  POM was studied in 12 different ILs with a range of different anions and cations. All RTILs showed reversible reduction processes corresponding

to successive one-electron additions, but some RTILs contained intrinsic impurities that made analysis after the second peak difficult. Where multiple reduction processes were visible, obvious trends in both the kinetics and thermodynamics were observed on varying the cation. Smaller peak-to-peak separations (faster kinetics) and lower energy barriers to reduction (smaller reduction potentials) were observed when the RTIL cation was an imidazolium, followed by ammonium  $\approx$  sulfonium, pyrrolidinium, then phosphonium. This suggests strong solvation and ion-pairing effects of the RTIL cation with the negatively charged POM reduction products. The RTIL that showed the fastest kinetics and lowest reduction potentials, ( $[C_2mim][FSI]$ ), was also used to study two phosphorus POMs, which both showed fast kinetics, but much more negative reduction potentials (by  $\sim 450 \text{ mV}$ ). Overall, this work shows that both the RTIL and the POM structures can result in differences in the kinetics and the thermodynamics of the electron transfer processes, and this should be considered when employing both of these promising materials for relevant electrochemical applications.

## Supplementary material

Description of the dissolution of POMs and their limited solubility in the different RTILs; data tables for peak-to-peak separations and reduction peak potentials for  $[S_2W_{18}O_{62}]^{4-}$  for all visible peaks in the 12 RTILs; cyclic voltammetry at different scan rates for five or six peaks in the RTILs, for the first two peaks and the first process, respectively, along with plots of peak current vs the square root of scan rate for the first reduction process for  $[S_2W_{18}O_{62}]^{4-}$  in all 12 RTILs; cyclic voltammetry at different scan rates for all visible peaks

for  $[P_2W_{18}O_{62}]^{6-}$  and  $[PW_{12}O_{40}]^{3-}$  in the RTIL  $[C_2mim][FSI]$ , along with plots of peak current vs the square root of scan rate for the first reduction peak; cyclic voltammetry in the sulfonium and an ammonium ionic liquid that overlapped with impurity peaks; digital simulation attempt to model the cyclic voltammetry for the four reduction processes of  $[PW_{12}O_{40}]^{3-}$  in  $[C_2mim][FSI]$ . This information is available on the Journal's website. Supplementary material is available [online](#).

## References

- [1] Pope MT. Heteropoly and Isopoly Oxometalates. Springer-Verlag: Berlin, Germany; 1983.
- [2] Borrás-Almenar JJ, Coronado E, Müller A, Pope MT. Polyoxometalate Molecular Science. Springer: Netherlands; 2003.
- [3] Roberts AP. Polyoxometalates: Properties, Structure and Synthesis. NOVA Science Publishers: New York, NY, USA; 2016.
- [4] Eldik Rv, Cronin L. Polyoxometalate Chemistry. Academic Press: Cambridge, MA, USA; 2017.
- [5] Sadakane M, Steckhan E. Electrochemical properties of polyoxometalates as electrocatalysts. *Chem Rev* 1998; 98: 219–238. doi:10.1021/cr960403a
- [6] Ueda T. Electrochemistry of polyoxometalates: from fundamental aspects to applications. *ChemElectroChem* 2018; 5: 823–838. doi:10.1002/celec.201701170
- [7] Nakajima K, Eda K, Himeno S. Effect of the central oxoanion size on the voltammetric properties of Keggin-type  $[XW_{12}O_{40}]^{n-}$  ( $n = 2-6$ ) complexes. *Inorg Chem* 2010; 49: 5212–5215. doi:10.1021/ic1003353
- [8] Maeda K, Katano H, Osakai T, Himeno S, Saito A. Charge dependence of one-electron redox potentials of Keggin-type heteropolyoxometalate anions. *J Electroanal Chem* 1995; 389: 167–173. doi:10.1016/0022-0728(95)03872-E
- [9] Hallett JP, Welton T. Room-temperature ionic liquids: solvents for synthesis and catalysis. *Chem Rev* 2011; 111: 3508–3576. doi:10.1021/cr1003248
- [10] Armand M, Endres F, MacFarlane DR, Ohno H, Scrosati B. Ionic-liquid materials for the electrochemical challenges of the future. *Nat Mater* 2009; 8: 621–629. doi:10.1038/nmat2448
- [11] Galiński M, Lewandowski A, Stepniak I. Ionic liquids as electrolytes. *Electrochim Acta* 2006; 51: 5567–5580. doi:10.1016/j.electacta.2006.03.016
- [12] Rogers RD, Seddon KR. Ionic liquids – solvents of the future? *Science* 2003; 302: 792–793. doi:10.1126/science.1090313
- [13] Wasserscheid P, Keim W. Ionic liquids – new “solutions” for transition metal catalysis. *Angew Chem Int Ed* 2000; 39: 3772–3789. doi:10.1002/1521-3773(20001103)39:21 <3772::AID-ANIE3772>3.0.CO;2-5
- [14] Fu H, Qin C, Lu Y, Zhang ZM, Li YG, Su ZM, Li WL, Wang EB. Electron-nuclear dynamics in molecular harmonic generation driven by a plasmonic nonhomogeneous field. *Angew Chem Int Ed* 2012; 51: 7985–7989. doi:10.1002/anie.201202994
- [15] Ahmed E, Ruck M. Ionothermal synthesis of polyoxometalates. *Angew Chem Int Ed* 2012; 51: 308–309. doi:10.1002/anie.201107014
- [16] Martinetto Y, Pégot B, Roch-Marchal C, Cottyn-Boitte B, Floquet S. Designing functional polyoxometalate-based ionic liquid crystals and ionic liquids. *Eur J Inorg Chem* 2020; 2020: 228–247. doi:10.1002/ejic.201900990
- [17] Zhang J, Bond AM, MacFarlane DR, Forsyth SA, Pringle JM, Mariotti AWA, Glowinski AF, Wedd AG. Voltammetric studies on the reduction of polyoxometalate anions in ionic liquids. *Inorg Chem* 2005; 44: 5123–5132. doi:10.1021/ic050032t
- [18] Zhang J, Bhatt AI, Bond AM, Wedd AG, Scott JL, Strauss CR. Voltammetric studies of polyoxometalate microparticles in contact with the reactive distillable ionic liquid DIMCARB. *Electrochim Commun* 2005; 7: 1283–1290. doi:10.1016/j.elecom.2005.09.008
- [19] Chiang MH, Dzielawa JA, Dietz ML, Antonio MR. Redox chemistry of the Keggin heteropolyoxotungstate anion in ionic liquids. *J Electroanal Chem* 2004; 567: 77–84. doi:10.1016/j.jelechem.2003.11.062
- [20] Reichardt C, Welton T. Solvents and Solvent Effects in Organic Chemistry, 4th edn. Wiley-VCH: Weinheim, Germany; 2010.
- [21] Himeno S, Takamoto M. Difference in voltammetric properties between the Keggin-type  $[XW_{12}O_{40}]^{n-}$  and  $[XMo_{12}O_{40}]^{n-}$  complexes. *J Electroanal Chem* 2002; 528: 170–174. doi:10.1016/S0022-0728(02)00901-4
- [22] Maeda K, Himeno S, Osakai T, Saito A, Hori T. A voltammetric study of Keggin-type heteropolyoxometalate anions. *J Electroanal Chem* 1994; 364: 149–154. doi:10.1016/0022-0728(93)02936-C
- [23] Ueda T, Kodani K, Ota H, Shiro M, Guo S-X, Boas JF, Bond AM. Voltammetric and spectroscopic studies of  $\alpha$ - and  $\beta$ - $[PW_{12}O_{40}]^{3-}$  polyoxometalates in neutral and acidic media: structural characterization as their  $[(n-Bu_4N)_3][PW_{12}O_{40}]$  salts. *Inorg Chem* 2017; 56: 3990–4001. doi:10.1021/acs.inorgchem.6b03046
- [24] Ueda T, Ohnishi M, Kawamoto D, Guo S-X, Boas JF, Bond AM. Voltammetric behavior of 1- and 4- $[S_2V^{IV}W_{17}O_{62}]^{5-}$  in acidified acetonitrile. *Dalton Trans* 2015; 44: 11660–11668. doi:10.1039/C5DT01530H
- [25] Rahman MA, Gundry L, Ueda T, Bond AM, Zhang J. Electrode material dependence, ion pairing, and progressive increase in complexity of the  $\alpha$ - $[S_2W_{18}O_{62}]^{4-5-6-7-8-9-10-}$  reduction processes in acetonitrile containing  $[n-Bu_4N][PF_6]$  as the supporting electrolyte. *J Phys Chem C* 2020; 124: 16032–16047. doi:10.1021/acs.jpcc.0c04735
- [26] Ishida H, Azuma S, Yamasaki N, Kurita H, Hasegawa T, Ogo S, Ueda T. Polyoxometalates in imidazolium-based ionic liquids: acceptor number and polarity estimated from their voltammetric behaviour. *Anal Sci* 2021; 37: 1131–1137. doi:10.2116/analsci.20P412
- [27] Anwar N, Armstrong G, Laffir F, Dickinson C, Vagin M, McCormac T. Redox switching of polyoxometalate-doped polypyrrole films in ionic liquid media. *Electrochim Acta* 2018; 265: 254–258. doi:10.1016/j.electacta.2017.12.101
- [28] Nikitina VA, Gruber F, Jansen M, Tsirlina GA. Subsequent redox transitions as a tool to understand solvation in ionic liquids. *Electrochim Acta* 2013; 103: 243–251. doi:10.1016/j.electacta.2013.04.069
- [29] Fedorov MV, Kornyshev AA. Ionic liquids at electrified interfaces. *Chem Rev* 2014; 114: 2978–3036. doi:10.1021/cr400374x
- [30] Hayes R, Warr GG, Atkin R. Structure and nanostructure in ionic liquids. *Chem Rev* 2015; 115: 6357–6426. doi:10.1021/cr500411q
- [31] Nishi N, Uchiyashiki J, Ikeda Y, Katakura S, Oda T, Hino M, Yamada NL. Potential-dependent structure of the ionic layer at the electrode interface of an ionic liquid probed using neutron reflectometry. *J Phys Chem C* 2019; 123: 9223–9230. doi:10.1021/acs.jpcc.9b01151
- [32] Cruz H, Gomes N, Mirante F, Balula SS, Branco LC, Gago S. Polyoxometalates-based ionic liquids (POMs-ILs) for electrochemical applications. *ChemistrySelect* 2020; 5: 12266–12271. doi:10.1002/slct.202002976
- [33] Bernardini G, Wedd AG, Zhao C, Bond AM. Photochemical oxidation of water and reduction of polyoxometalate anions at interfaces of water with ionic liquids or diethylene glycol. *Proc Natl Acad Sci USA* 2012; 109: 11552–11557. doi:10.1073/pnas.1203818109
- [34] Wang MY, Song QW, Ma R, Xie JN, He LN. Efficient conversion of carbon dioxide at atmospheric pressure to 2-oxazolidinones promoted by bifunctional Cu(ii)-substituted polyoxometalate-based ionic liquids. *Green Chem* 2016; 18: 282–287. doi:10.1039/C5GC02311D
- [35] Herrmann S, Kostrzewa M, Wierschem A, Streb C. Polyoxometalate ionic liquids as self-repairing acid-resistant corrosion protection. *Angew Chem Int Ed* 2014; 53: 13596–13599. doi:10.1002/anie.201408171
- [36] Misra A, Franco Castillo I, Müller DP, González C, Eyssautier-Chuine S, Ziegler A, de la Fuente JM, Mitchell SG, Streb C. Polyoxometalate-ionic liquids (POM-ILs) as anticorrosion and antibacterial coatings for natural stones. *Angew Chem Int Ed* 2018; 57: 14926–14931. doi:10.1002/anie.201809893
- [37] Himeno S, Tatewaki H, Hashimoto M. Synthesis, structure, and characterization of an  $\alpha$ -Dawson-type  $[S_2W_{18}O_{62}]^{4-}$  complex. *Bull Chem Soc Jpn* 2001; 74: 1623–1628. doi:10.1246/bcsj.74.1623
- [38] Ueda T, Suzuki M, Toya T. The enhancement of the formation of Wells–Dawson-type polyoxometalates by the addition of high

- concentrations of LiCl. *J Clust Sci* 2015; 27: 501–511. doi:10.1007/s10876-015-0946-y
- [39] Zhang J, Bond AM. Conditions required to achieve the apparent equivalence of adhered solid- and solution-phase voltammetry for ferrocene and other redox-active solids in ionic liquids. *Anal Chem* 2003; 75: 2694–2702. doi:10.1021/ac026329f
- [40] Doblínger S, Donati TJ, Silvester DS. Effect of humidity and impurities on the electrochemical window of ionic liquids and its implications for electroanalysis. *J Phys Chem C* 2020; 124: 20309–20319. doi:10.1021/acs.jpcc.0c07012
- [41] Bengio D, Mendes E, Pellet-Rostaing S, Moisy P. Electrochemical behavior of platinum and gold electrodes in the aprotic ionic liquid *N,N*-Trimethylbutylammonium bis(trifluoromethanesulfonyl)imide. *J Electroanal Chem* 2018; 823: 445–454. doi:10.1016/j.jelechem.2018.06.034
- [42] Sas OG, Domínguez I, González B, Domínguez Á. Liquid-liquid extraction of phenolic compounds from water using ionic liquids: literature review and new experimental data using [C<sub>2</sub>mim]FSI. *J Environ Manage* 2018; 228: 475–482. doi:10.1016/j.jenvman.2018.09.042
- [43] Gaciño FM, Regueira T, Lugo L, Comuñas MJP, Fernández J. Influence of molecular structure on densities and viscosities of several ionic liquids. *J Chem Eng Data* 2011; 56: 4984–4999. doi:10.1021/je200883w
- [44] Gau V, Ma S-C, Wang H, Tsukuda J, Kibler J, Haake DA. Electrochemical molecular analysis without nucleic acid amplification. *Methods* 2005; 37: 73–83. doi:10.1016/j.jmeth.2005.05.008
- [45] Bard AJ, Faulkner LR. *Electrochemical Methods: Fundamentals and Applications*, 2nd edn. Wiley: Hoboken, NJ, USA; 2001.
- [46] Thakurathi M, Gurung E, Cetin MM, Thalangaarachchige VD, Mayer MF, Korzeniewski C, Quitevis EL. The Stokes–Einstein equation and the diffusion of ferrocene in imidazolium-based ionic liquids studied by cyclic voltammetry: effects of cation ion symmetry and alkyl chain length. *Electrochim Acta* 2018; 259: 245–252. doi:10.1016/j.electacta.2017.10.149
- [47] Barrosse-Antle LE, Bond AM, Compton RG, O'Mahony AM, Rogers EI, Silvester DS. Voltammetry in room temperature ionic liquids: comparisons and contrasts with conventional electrochemical solvents. *Chem Asian J* 2010; 5: 202–230. doi:10.1002/asia.200900191
- [48] Kang C, Lee J, Silvester DS. Electroreduction of 2,4,6-trinitrotoluene in room temperature ionic liquids: evidence of an EC<sub>2</sub> mechanism. *J Phys Chem C* 2016; 120: 10997–11005. doi:10.1021/acs.jpcc.6b03018
- [49] Nazet A, Sokolov S, Sonnleitner T, Makino T, Kanakubo M, Buchner R. Densities, viscosities, and conductivities of the imidazolium ionic liquids [Emim][Ac], [Emim][FAP], [Bmim][BETI], [Bmim][FSI], [Hmim][TFSI], and [Omim][TFSI]. *J Chem Eng Data* 2015; 60: 2400–2411. doi:10.1021/acs.jced.5b00285
- [50] Machanová K, Boisset A, Sedláková Z, Anouti M, Bendová M, Jacquemin J. Thermophysical properties of ammonium-based bis((trifluoromethyl)sulfonyl)imide ionic liquids: volumetric and transport properties. *J Chem Eng Data* 2012; 57: 2227–2235. doi:10.1021/je300108z
- [51] Klein JM, Squire H, Gurkan B. Electroanalytical investigation of the electrode–electrolyte interface of quaternary ammonium ionic liquids: impact of alkyl chain length and ether functionality. *J Phys Chem C* 2020; 124: 5613–5623. doi:10.1021/acs.jpcc.9b08016
- [52] Evans RG, Klymenko OV, Saddoughi SA, Hardacre C, Compton RG. Electroreduction of oxygen in a series of room temperature ionic liquids composed of Group 15-centered cations and anions. *J Phys Chem B* 2004; 108: 7878–7886. doi:10.1021/jp031309i
- [53] Silvester DS, Uprety S, Wright PJ, Massi M, Stagni S, Muzzioli S. Redox properties of a rhenium tetrazolato complex in room temperature ionic liquids: assessing the applicability of the Stokes–Einstein equation for a metal complex in ionic liquids. *J Phys Chem C* 2012; 116: 7327–7333. doi:10.1021/jp3007975
- [54] Bentley CL, Li J, Bond AM, Zhang J. Mass-transport and heterogeneous electron-transfer kinetics associated with the ferrocene/ferrocenium process in ionic liquids. *J Phys Chem C* 2016; 120: 16516–16525. doi:10.1021/acs.jpcc.6b05545
- [55] De Vreese P, Haerens K, Matthijs E, Binnemans K. Redox reference systems in ionic liquids. *Electrochim Acta* 2012; 76: 242–248. doi:10.1016/j.electacta.2012.04.108
- [56] Bhattacharjee A, Luís A, Santos JH, Lopes-da-Silva JA, Freire MG, Carvalho PJ, Coutinho JAP. Thermophysical properties of sulfonium- and ammonium-based ionic liquids. *Fluid Phase Equilib* 2014; 381: 36–45. doi:10.1016/j.fluid.2014.08.005
- [57] Shoup D, Szabo A. Chronoamperometric current at finite disk electrodes. *J Electroanal Chem Interfacial Electrochem* 1982; 140: 237–245. doi:10.1016/0022-0728(82)85171-1
- [58] Umecky T, Kanakubo M, Ikushima Y. Self-diffusion coefficients of 1-butyl-3-methylimidazolium hexafluorophosphate with pulsed-field gradient spin-echo NMR technique. *Fluid Phase Equilib* 2005; 228–229: 329–333. doi:10.1016/j.fluid.2004.08.006
- [59] Compton RG, Banks CE. *Understanding Voltammetry*, 2nd edn. Imperial College Press: London, UK; 2010
- [60] Mashkina E, Bond AM, Simonov AN. Limitations in electrochemical determination of mass-transport parameters: implications for quantification of electrode kinetics using data optimisation methods. *Aust J Chem* 2017; 70: 990–996. doi:10.1071/CH17241
- [61] Buzzeo MC, Klymenko OV, Wadhawan JD, Hardacre C, Seddon KR, Compton RG. Voltammetry of oxygen in the room-temperature ionic liquids 1-ethyl-3-methylimidazolium bis((trifluoromethyl)sulfonyl)imide and hexyltriethylammonium bis((trifluoromethyl)sulfonyl)imide: one-electron reduction to form superoxide. Steady-state and transient behavior in the same cyclic voltammogram resulting from widely different diffusion coefficients of oxygen and superoxide. *J Phys Chem A* 2003; 107: 8872–8878. doi:10.1021/jp0304834

**Data availability.** The data that support this study will be shared upon reasonable request to the corresponding author.

**Conflicts of interest.** The authors declare no conflicts of interest.

**Declaration of funding.** This work was supported by the JSPS Core-to-Core Collaboration in Advanced Research Network, International Network on Polyoxometalate Science for Advanced Functional Energy Materials, the Cooperative Research Program of Network Joint Research Center for Materials and Devices, and Takahashi Industrial and Economic Research Foundation for TU. In addition, SA thanks 'TOBITATE!' Leap for tomorrow! Study Abroad Initiative Young Ambassador Program for financial support for his visit to Curtin University.

**Acknowledgements.** DSS thanks the Australian Research Council for a Future Fellowship (FT170100315) and the Chemistry department at Curtin University for the summer scholarship for JIP.

#### Author affiliations

<sup>A</sup>School of Molecular and Life Sciences, Curtin University, GPO Box U1987, Perth, WA 6845, Australia.

<sup>B</sup>Graduate School of Integrated Arts and Sciences, Kochi University, Kochi 780-8520, Japan.

<sup>C</sup>Department of Marine Resource Science, Faculty of Agriculture and Marine Sciences, Kochi University, Nankoku 783-8520, Japan.

<sup>D</sup>Centre for Advanced Marine Core Research, Kochi University, Nankoku 783-8502, Japan.